Excitation of broadband surface plasmon polaritons: Plasmonic continuum spectroscopy

A. Bouhelier and G. P. Wiederrecht
Chemistry Division and Center for Nanoscale Materials, Argonne National Laboratory, Argonne, Illinois 60439, USA
(Received 21 December 2004; revised manuscript received 11 February 2005; published 11 May 2005)

The excitation of surface plasmon polaritons in a thin metal film is extremely sensitive to the surrounding dielectric environment. We introduce here a far-field method to directly observe surface plasmon propagation and demonstrate that the lateral intensity decay length is affected by a change of the interface properties. The method relies on the detection of the intrinsic lossy modes associated with plasmon propagation in thin films. We also introduce a method to excite a broad spectral distribution of surface plasmons simultaneously throughout the visible spectrum allowing a unique form of surface plasmon-based spectroscopy.

DOI: 10.1103/PhysRevB.71.195406 PACS number(s): 73.20.Mf, 78.66.−w, 42.82.Gw, 07.60.Pb

I. INTRODUCTION

Surface plasmon resonance spectroscopy (SPR) has been extensively studied in the past, providing quantitative and qualitative analyses in analytical chemistry,[1] biochemistry,[2] and physics applications.[3] Surface plasmon polaritons (SPPs) are known solutions of Maxwell's equations applied along an interface between a medium with a negative permittivity, i.e., a metal and a dielectric. Being an interface phenomenon, SPPs are extremely sensitive to the dielectric environment surrounding that interface. The resonance condition to excite SPPs is governed by a dispersion relation between the wave vector of the incident light and the energy of the SPPs. For real metals, where the metal permittivity ϵ_m is a complex quantity ($\epsilon_m = \epsilon_m' + i\epsilon_m''$), the dispersion relation $k(\omega)$ is composed of a real term $k'(\omega)$ and an imaginary term $k''(\omega)$.

In the classical embodiment of SPR spectroscopy, i.e., the Kretschmann configuration,[4] a metal-coated prism is used to reflect an incoming light beam with a total internal reflection geometry. For a given excitation wavelength, the dispersion relation of the SPPs must be fulfilled in order to excite the SPP resonance. This is achieved by adjusting the angle of incidence of the incoming light. Alternatively, constant-angle sensors use monochromators to match the resonant energy.[5] At the resonance condition, the light is absorbed by the metal film in the form of SPPs. The signature of SPP excitation results in a decrease of the intensity reflected from the metal surface. Plotting the normalized intensity of the reflected beam against the angle of incidence or incoming wavelength reveals the resonance in the form of a SPR intensity minimum. Monitoring the shift of the SPR minimum upon changes of the dielectric environment such as a molecular adsorption on the metal film, is the basis for commercial SPR spectroscopy. For noble metals such as gold and silver, $k'(\omega) \gg k''(\omega)$ in the visible part of the spectrum and the position of the reflected minimum is mostly affected by modifications of $k'(\omega)$.

With the increasing trend towards the miniaturization of photonic circuits, it was realized recently that the confined nature of surface plasmons and their relatively long propagation length make them suitable for integration in metallic planar circuitry designs.[6] Due to the evanescent nature of the SPP field traveling at the metal/air interface, near-field techniques are instrumental in the observation of SPP propagation.[7–10] An increasing number of near-field studies deal with the interaction of SPPs with film defects or structures fabricated on metal films.[11–18] The lateral decay of the surface plasmon traveling in the film is a measure of the ideality of the electron gas and is mainly influenced by the imaginary part $k''(\omega)$ of the dispersion.[3] Experimentally, the SPP lateral damping mechanisms and the effect of adsorbates on the propagation length of the SPPs were originally studied in the infrared region[19–21] and more recently at the 632-nm laser frequency in the visible.[22] In this work, we show how intrinsic and extrinsic losses affect the SP lateral decay length throughout the visible part of the spectrum. We unambiguously demonstrate the influence of small dielectric changes on the attenuation of the SPPs. To this end, we developed a unique scheme to excite surface plasmon waves and to directly visualize their lateral intensity distributions. Instead of reconstructing a two-dimensional map of the plasmon intensity with the help of near-field techniques, we directly observe the SPP lateral distribution by detecting SPP's intrinsic radiation losses inherent to their existence in thin metal films. The proposed technique relaxes some of the limitations of classical SPR imposed by the dispersion relation such as constant-angle or constant-wavelength excitation. Our new approach of plasmonic continuum spectroscopy (PCS) allows us to excite simultaneously a white-light continuum of SPPs throughout the visible spectral region. Broadband surface plasmon polaritons have potential for the investigation of wavelength-sensitive planar photonic devices or for the spectral study of adsorbates on metal films, areas of technological and basic science interest.

II. EXPERIMENTAL CONFIGURATION

For a thin metal film (permittivity ϵ_m) bounded by two different dielectric media (permittivities ϵ_1 and ϵ_2) there are a total of four solutions to the dispersion relations,[23] two of which are nonradiative modes existing at each of the interfaces. Figure 1(a) shows the mode solutions for a wave bound at the interface ϵ_m/ϵ_1. The wave amplitudes associated with these bounded modes are exponentially decaying across the metal and the dielectric medium. As the field penetrates to the opposite interface (ϵ_m/ϵ_2), it couples into radiative leaky waves propagating in the dielectric that are the

 ©2005 The American Physical Society

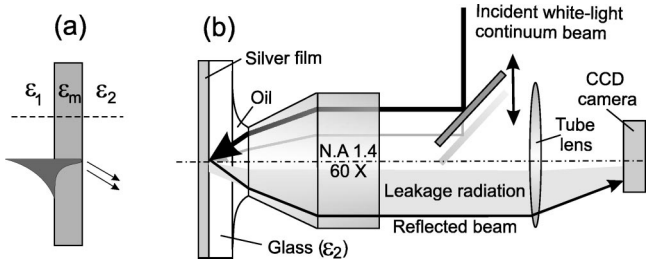

FIG. 1. (a) Field distribution of a surface plasmon mode bound at the metal/air interface (ϵ_m/ϵ_1) and the leakage radiation in medium ϵ_2. (b) Schematic of the excitation of a white-light continuum of surface plasmons and their observation through detection of the leakage radiation using an index-matched oil immersion lens.

remaining solutions of the dispersion relations. As the film thickness increases, the waves confined at the interfaces eventually decouple, and the dispersion relations of the structure are similar to the ones describing surface waves at the interface between semi-infinite media.

In SPR techniques where the excitation area roughly compares with the SPP propagation length, this lossy leakage radiation (LR) interferes destructively with the incoming excitation light and cannot be detected.[3] However, if the excitation area is significantly smaller than the lateral spread of the surface plasmons, LR can be observed.[3,10,14] The observation of LR gives a direct measurement of the nonradiative surface plasmon traveling at the opposite interface. The intensity of the losses, at a given lateral position in the film, is proportional to that of the SPP at the same position.[10]

Figure 1(b) describes the experimental apparatus used to excite a white-light continuum of SPPs and the detection of the associated leakage radiation. SPPs were excited in a very similar manner to the Kretschmann configuration. Unlike the conventional SPR apparatus, we did not use a right-angle prism to satisfy the total internal reflection and the SPP resonance requirements. Instead, a high-numerical aperture oil-immersion objective (N.A.=1.4) was used.[24]

There are several key advantages for using an oil-immersion lens to excite surface plasmons over the standard prism. First, in order to visualize the leakage radiation, the SPP excitation area must be smaller than the SPP propagation length. This is achieved by focusing the illumination beam to a small area. As a result of the focusing, a broad distribution of rays or wave vectors are incident on the glass/silver interface. For a given wavelength, a resonant wave vector will be responsible for SPP excitation, while the others will be reflected or transmitted through the film. However, if the illumination light is composed of a white-light continuum, virtually all wave vectors will be able to couple into SPPs providing that the angular spread of the illumination beam is large enough to have all the resonance wave vectors of the continuum. The SPP excitation angles for wavelengths throughout the visible are confined within a few degrees around 45°. Therefore, if the full N. A. of the objective is used, only a small fraction of the light will be converted into SPPs and the overwhelming remaining part will be either reflected from the film or transmitted through it. Instead of completely filling the back-aperture of the lens, a small beam of collimated white-light radiation was adjusted within the back aperture of the lens as depicted in Fig. 1(b). The angle of the beam emerging from the lens and the angular spread was controlled by adjusting the beam position with respect to the optical axis. The broadband excitation and emission of surface plasmons was reported in the past through fluorescent near-field coupling.[25] However, the spectral content of the surface plasmon polaritons in that particular study was limited by the fluorescent response of the photoresist employed.

Another advantage of the high N. A. immersion lens is its ability to capture the SPP's leakage radiation. The LR is characterized by a well-defined emission angle θ_{SP} for every wavelength that is greater than the critical angle in the glass. Therefore, elements in optical contact with the substrate are necessary to avoid total internal reflection of LR within the glass substrate. The objective is part of a conventional inverted optical microscope focused on the metal/glass interface and is used both for SPP excitation and LR detection. The leakage radiation was recorded and imaged by a CCD camera placed in the image plane of the microscope as depicted in Fig. 1(b).

The white-light continuum was produced by the output of a Coherent MIRA regeneratively amplified Ti:sapphire laser system. The continuum is created through well-known methods, in particular by focusing the 800-nm pulses into a small piece of sapphire (50 fs/pulse at 250 kHz). The white light produced in this manner is generally easier to manipulate, collimate, and focus than other typical white light sources. The white-light was spatially filtered by coupling the beam into a ~ 5 μm diameter optical fiber. A collimating objective (N.A.=0.4) was used against the 0.1 N. A. of the fiber to produce a 1.5 mm diameter collimated white-light beam. The polarization of the continuum beam was controlled by a combination of a multiwavelength wave plate and Glan-Thompson polarizer. The asymmetric plasmonic films were produced by thermally evaporating thin silver films on cleaned glass cover slips. We investigated films with a silver layer of 30, 40, 50, and 70 nm. The thickness and the roughness characteristics of the films were checked by atomic force microscopy (AFM).

III. SURFACE PLASMON RAINBOW JET

Figure 2(a) shows the leakage radiation emitted at the metal/glass interface by a white-light continuum of surface plasmons traveling at the air/metal interface. The excitation light was *p* polarized to match the polarization of the surface waves. The illumination spot reflected at the glass/metal interface can be seen in Fig. 2(a) as a bright white circular spot in the right-hand side of the image. The excitation spot is about 3 μm at full-width at half-maximum. To the left of that region, a rainbow jet extends along the in-plane wave vector ($\vec{k}$) corresponding to the direction of the excitation wave vector projected on the surface of the film.

The spectral intensity distribution of the SPP jet can be understood from the dispersion curve of the interface $k(\omega)$. For the red part of the spectrum, the dispersion curve follows very closely the light line resulting in large group velocities $d\omega/dk$ of the waves. The intrinsic losses given by the imagi-

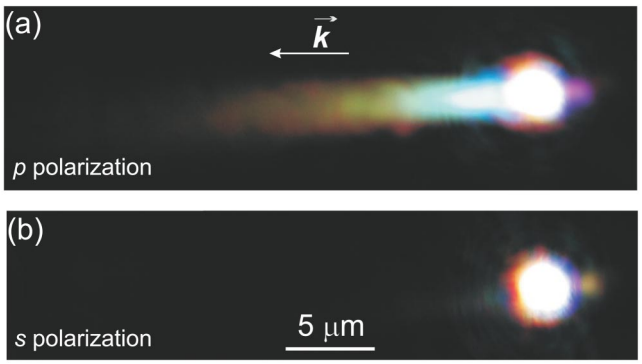

FIG. 2. (Color online) Surface plasmon rainbow jet emitted from a 50-nm-thick silver film. (a) Leakage radiation intensity distribution for a *p* polarized white-light continuum excitation beam. The surface plasmons form a rainbow jet as they propagate away from the focal spot. (b) Control experiment with an excitation beam that is *s* polarized.

nary part of the complex permittivity ϵ_m'' in the metal are small and the SPP propagates for relatively long distances on the metal film. For smaller wavelengths, the curve flattens out to reach asymptotically $\omega_p/\sqrt{2}$, where ω_p is the plasma frequency of the metal. As ϵ_m'' increases in these excitation frequencies, the group velocity is reduced to smaller quantities. The consequence of this behavior can be observed as a dispersion of the propagation length of the various spectral components composing the surface plasmon continuum. The blue part of the spectrum tends to be more confined to the excitation spot, whereas the longer wavelengths propagate further on the film surface as shown in Fig. 2(a). A control experiment is shown in Fig. 2(b) where an *s*-polarized excitation beam was used. The jet is no longer observed for this case and confirms that the signal observed for *p*-polarized excitation is due to the SPP's leakage radiation. The small protrusions situated on the right side of the excitation area are ghost reflections originating from the Glan-Thompson polarizer.

IV. SURFACE PLASMON LATERAL DECAY LENGTH

The decay lengths of the different spectral components of the surface plasmon continuum were quantitatively measured by replacing the imaging CCD camera of Fig. 1(b) by a spectrograph coupled to a nitrogen-cooled CCD chip with 256×1064 $(x\times y)$ pixels. The image plane of the SPP rainbow jet was placed in the entrance slit of the spectrograph and dispersed on the CCD chip. The main axis of the jet was oriented with the slit axis x so that a spectrum recorded at a given pixel-line x dispersed the spectral information of the intensity across the jet. Spectra of the rainbow jet were then acquired by incrementing x along the propagation direction (the distance between two x lines of pixels corresponded to ~370 nm at the sample plane). Normalizing the intensity of the spectra for a given wavelength and plotting the values as a function of distance reveals the decay rate of the SP intensity. Such a plot is shown in Fig. 3(a) in a semilogarithmic scale for four wavelengths (600, 550, 500, and 475 nm). The experimental data are well characterized by a single exponential decay, and the SPP intensity I_{SP} can be expressed as $I_{SP}\sim e^{-L_{SP}/x_s}$. L_{SP} and x_s are the decay length and the lateral distance from the source, respectively.

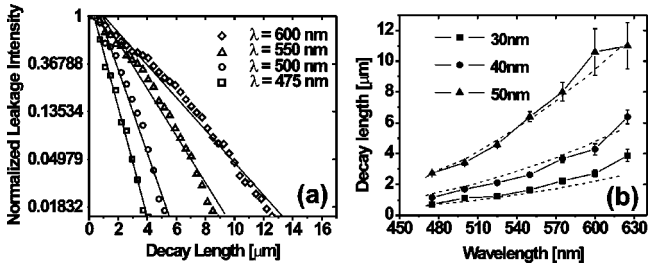

FIG. 3. (a) Semilogarithmic plot of the surface plasmon leakage radiation decay for four wavelengths 600 nm (diamonds), 550 nm (triangles), 500 nm (circles), and 475 nm (squares). The solid curves represent single exponential decays fitted to the data. (b) Experimental surface plasmon decay length L_{SP} (data points) as a function of the SPP wavelength for film thickness of 30 nm (rectangles), 40 nm (circles), and 50 nm (triangles). The dashed curves are the computed decay length for three different film thicknesses.

The data points in Fig. 3(b) show the results of the exponential fitting procedure as a function of wavelength for three different thicknesses of the silver film. The error bars in the graph represent the confidence margin of the exponential fits and do not include the uncertainty of the film thickness. As expected from the wavelength dependence of the silver permittivity and from Fig. 2(a), the longer propagation distances are achieved for the longer excitation wavelength. The values of L_{SP} are consistent with reported propagation distances for single wavelength measurements.[7,14] Additionally, Fig. 3(b) demonstrates that the decay length L_{SP} of the SPP, for a given wavelength, shows a dispersive behavior as a function of film thickness. This thickness dispersion was theoretically predicted[23] and can be understood in terms of coupling efficiency. The amplitude of the SPP field at the air/metal interface is exponentially decaying across the metal layer and is coupled into leakage radiation in the opposite medium (glass in the present case). As the thickness of the metal layer is decreased, the coupling efficiency is increased, and radiation loss dominates the wave attenuation.

For an asymmetric structure, the imaginary part $k''(\omega)$ of the dispersion relation is composed of two terms $k''(\omega)=k_{\text{int}}''+k_{\text{rad}}''$, where k_{int}'' represents the imaginary part of the dispersion relation for an interface between two semi-infinite media and k_{rad}'' is an additional radiative contribution due to the small thickness of the film:[26]

$$k_{\text{int}}'' = \left(\frac{2\pi}{\lambda}\right)\frac{\epsilon_m''}{2\epsilon_m'^2}\left(\frac{|\epsilon_m'|}{|\epsilon_m'|-1}\right)^{3/2}, \tag{1}$$

$$k_{\text{rad}}'' = \left(\frac{2\pi}{\lambda}\right)\frac{\beta}{|\epsilon_m'|+1}\left(\frac{|\epsilon_m'|}{|\epsilon_m'|-1}\right)^{3/2}\exp\left(-\frac{4\pi d|\epsilon_m'|}{\lambda\sqrt{|\epsilon_m'|-1}}\right) \tag{2}$$

with

$$\beta = \frac{2\epsilon_2\sqrt{|\epsilon_m'|(\epsilon_2-1)-\epsilon_2}}{\epsilon_2^2+|\epsilon_m'|(\epsilon_2-1)-\epsilon_2}. \tag{3}$$

In the equations above, ϵ_2 is the permittivity of the glass, d is the thickness of the metal film and λ is the SPP wavelength. The lateral attenuation L_{SP} of the SPP waves is inversely proportional to $k''(\omega)$ $[L_{SP}=1/2k''(\omega)]$. In addition to these intrinsic damping processes (dissipation in the metal and radiation), the surface roughness of the film also contributes to the attenuation of the SPP.[27] The inhomogeneities of the film damp the traveling SPP through roughness-induced radiation loss into the upper medium (air in our case) and through scattering into other plasmon states. The mean-free paths L^r_{scat} and L^r_{rad} of the waves are written in the forms[27]

$$L^r_{scat} = \frac{2}{3}\frac{\lambda^5|\epsilon_m|}{(2\pi)^5\delta^2\sigma^2} \tag{4}$$

and

$$L^r_{rad} = \frac{3}{4}\frac{\lambda^5\sqrt{|\epsilon_m|}}{(2\pi)^5\delta^2\sigma^2}. \tag{5}$$

The parameters δ and σ are quantities defined by the specific roughness of the film. δ is a measure of the average roughness of the surface and was estimated by AFM ($\delta \sim 3$–6 nm). σ is called the transverse correlation length and is a measure of the randomness of the roughness distribution.[27] For vanishing σ, the film has a complete random roughness distribution. Assuming a Gaussian model for the film inhomogeneities, σ was estimated at around 50 nm by autocorrelating a 2 μm$\times$2 μm AFM topographical image of the surface.

We computed the values of k''_{int} and k''_{rad} [Eq. (2) and Eq. (3)] from the published values of the silver permittivity[3] and estimated the value of the wavelength-dependent SPP decay lengths for the three experimental film thicknesses. We included in the calculation of L_{SP}, the roughness-induced attenuation of the SPP wave taking into account the experimental values of δ and σ using the following relation:[27]

$$\frac{1}{L_{SP}} = \frac{1}{2(k''_{int}+k''_{rad})} + \frac{1}{L^r_{scatt}} + \frac{1}{L^r_{rad}}. \tag{6}$$

The sum of these intrinsic and extrinsic damping contributions are plotted as dashed lines in Fig. 3(b). There is a fairly good agreement with the experimental decay length considering that no free parameters were used to fit the data. We note that the calculation of k''_{int} and k''_{rad} using permittivity values acquired by standard reflection measurements[28] gave a systematic overestimation of the decay length. Instead, we calculated L_{SP} with the silver permittivity measured by SPR spectroscopy[3] which gives a slightly higher imaginary component ϵ''_m and a better fit to our experimental data. It has to be emphasized here that the estimation of L^r_{scatt} and L^r_{rad} contributed only to a few percent of the total attenuation of the SPP wave. The major cause of the damping for the film thicknesses considered here comes from the radiation losses due to k''_{rad} and not from intrinsic absorption due to ϵ''_m (e.g., k''_{int}). For increasing film thickness, the intensity of the LR is drastically reduced. We were not able to observe the LR for a 70-nm-thick silver film. Reducing the effect of the LR by increasing the thickness of the films would result in a larger propagation distance mainly governed by k''_{int}. However, early studies with a Kretschmann configuration showed that there is an optimum film thickness for which the incoming incident light is efficiently coupled into surface plasmons at the metal/air interface.[3] Increasing the thickness would only reduces the SPP coupling efficiency. Therefore a trade off exists between large SPP propagation distances and incoming energy coupled into surface plasmons.

V. INFLUENCE OF MONOLAYER ADSORBATES

We then investigated how the surface plasmon decay lengths are altered with the addition of molecular adsorbates. Molecular adsorbates can alter the decay lengths through a change of the dielectric constant at the air/metal interface, or by altering the surface scattering of the plasmon through effects such as chemical interface damping.[29,30] This results from bonding and/or charge transfer interactions between the adsorbate and the metal. As a first step, we used classical thiol-based chemistry to modify the interface characteristics through the covalent bonding of the thiol to silver. Single monolayers of nonanethiol $C_9H_{20}S$ or dodecanethiol $C_{12}H_{26}S$ were self-assembled on a 40-nm-thick silver film. In order to reduce the effect of silver oxidation, we freshly prepared a silver film and cut it in three different pieces. Immediately after the evaporation, the three pieces were submerged in oxygen-free toluene. Two petri dishes containing undiluted solutions of the alkanethiols were prepared. The silver samples were then placed in the respective solutions and left to incubate for 24 h. The unmodified bare silver film was kept in toluene and used as a reference. The incubated films were then copiously rinsed with toluene to wash out unbound molecules. We performed AFM characterization on films prepared with the same procedure to verify the presence of the monolayer. We measured an increased roughness similar to the length of the molecules indicative of the monolayer formation. The films were then placed in our surface plasmon apparatus in order to assess the influence of the two different monolayers on the surface plasmon propagation. Figure 4 shows the result of the comparison between the unmodified silver film and the films with adsorbed nonanethiol and dodecanethiol. We omitted the error bars in the graph for the sake of clarity. They are comparable to the one in Fig. 3(b) for the 40-nm-thick film. Figure 4 shows that the surface plasmon decay length L_{SP} is influenced by the presence of a monolayer adsorbed on the silver surface. In the blue region, i.e., for short propagation distances, the difference between the bare silver film and the $C_9H_{20}S$ monolayer is comprised within the measurement errors. For larger propagation distances, the cumulative effect of the monolayer results in a noticeable damping of the lateral decay. For the $C_{12}H_{26}S$ monolayer, the SPP decay lengths are clearly lower than the one measured for the bare silver film. While the difference is small compared to the overall decay length, the measured variations for the long thiol chain exceed the magnitude of the error bars of the exponential fits. Control experiments with another set of silver films produced very similar variations in the decay lengths. The modification of the surface plasmon excitation conditions (resonant angle)

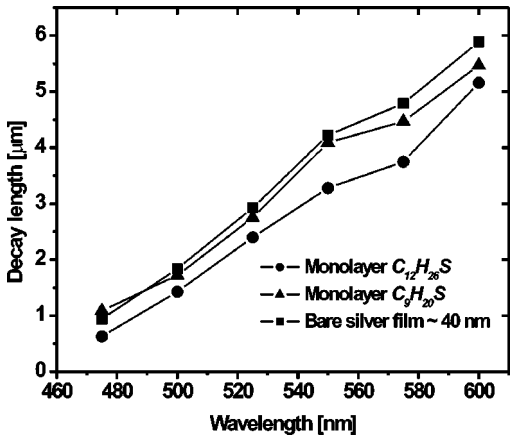

FIG. 4. Comparison of the wavelength dependence of the surface plasmon decay length between a bare 40-nm-thick silver film, a monolayer of nonanethiol ($C_9H_{20}S$), and a monolayer of dodecanethiol ($C_{12}H_{26}S$) adsorbed on the same silver film but at different locations, respectively. The error bars have been omitted for the sake of clarity and are comparable to the ones shown in Fig. 3(b).

upon the formation of a monolayer on the silver surface were experimentally observed before by SPR spectroscopy.[31] However, we believe that the influence of self-assembled monolayer adsorbates on the SPP propagation was never investigated before and is of importance for the emerging field of plasmonics. Our approach permits the differentiation on SPP propagation attenuation between monolayers with a length difference as small as three carbon atoms.

Figure 3(b) shows that slight variations in the film thickness could lead to rather large variations of L_{SP}. The uncertainty during two metal evaporations or the errors due to the AFM characterization for an apparent similar film thickness may result in different decay values. A good example of such variation can be seen by comparing the values of L_{SP} shown in Figs. 3(b) and 4 for two different 40-nm-thick films. This is particularly true in the 600-nm range, where only a 2 to 3 nm change in the film thickness can produce propagation distances variations of 2 μm or more. Therefore it is important to compare the influence of an interface change between films prepared simultaneously in order to reduce the experimental errors.

VI. MOLECULAR EXCITON: A PLASMONIC REJECTION FILTER

Next, we investigated the propagation losses of surface plasmon upon formation of molecular *J*-aggregates on the metal films. *J*-aggregates are characterized by a redshifted and sharp absorption band relative to the monomer band, a result of exciton delocalization over the molecular building blocks of the aggregate.[32–35] Molecular *J*-aggregates are a target for the organic component of heterostructures because they are well known for collective excitons with large oscillator strength, while their ease of oxidation makes them useful as sensitizers in the photographic process of electron injection into AgBr semiconductor particles. Additionally, they are of interest in many fields, such as modeling energy transfer, nonlinear optics, and solar photochemical energy conversion.[36–46]

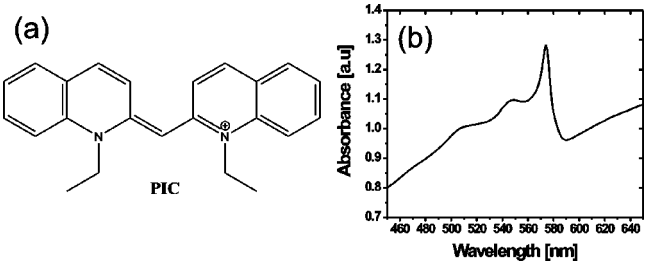

FIG. 5. (a) Atomic structure of a 1,1′-diethyl-2,2′-cyanine iodide molecule (PIC). (b) Absorbance spectrum of the *J* aggregate formed on a 40-nm-thick silver film. The exciton absorption peaks at 575 nm.

We used a very well-known *J*-aggregate consisting of 1,1′-diethyl-2,2′-cyanine iodide molecules (PIC), shown in Fig. 5(a). Our wide continuum of surface plasmon energy is well suited here to monitor the influence of this narrow absorption peak on L_{SP} as a function of wavelength. Resonant interactions of surface plasmons with dye monolayers have been studied in the past with SPR spectroscopy and demonstrated a strong influence of the dye on the SPP dispersion relation.[47,48] The nonradiative energy transfer of excited dye molecules on the metal surface was also studied by SPR spectroscopy and was shown to be strongly dependent on the metal-molecule separation.[49–51] In these studies, the molecules were systematically separated from the silver surface by organic spacers to allow the aggregates to form within a monolayer. We took a somewhat easier approach where a small volume of concentrated solution of PIC was simply deposited on a fresh 40-nm silver film and left to dry. The formation of the *J*-aggregates on the film was verified by absorption spectroscopy. The absorption spectrum is shown in Fig. 5(b). The exciton resonance absorption peaks at 575 nm and is in accordance with previous work.[52] The spectral feature on the high-energy side of the excitonic peak is the remaining molecular absorption of the dye molecules that did not contribute to the *J*-aggregate formation.

The wide spectrum of surface plasmons was excited in a region exposed to the *J*-aggregate and compared to an unmodified region of the silver film. The result of the comparison is shown in Fig. 6. The reference bare silver film (triangle) has a systematically larger SPP propagation length L_{SP} than the modified film. This is to be expected considering the sensitivity of the technique to the dielectric change at the metal surface (see Fig. 4). Additionally, the remaining molecular absorption also contributes to a reduction of L_{SP}. We observed fluorescence in the green-orange part of the spectrum that originates from the dye. However, the intensity of the fluorescence was systematically weaker than the leakage radiation intensity. At the exciton peak, the attenuation of the SPP is considerably decreased and is modified from 5 μm for the reference measurement to 0.5 μm. Due to the narrow spectral absorption, such attenuation would have been difficult to observe with standard single-wavelength SPP excitation methods. Our broad continuum of surface plasmons enabled us to perform this unique form of spectroscopy.

In the context of plasmonic integrated devices, the increased absorption due to a molecular exciton can be thought

of as an efficient notch filter for SPP frequencies within the resonance band. *J*-aggregates are commercially available with exciton peaks spanning the visible spectrum which would offer a wide selection of SPP filters.

The excitonic increased absorption is responsible for the dramatic reduction of the SPP decay length. From the theoretical point of view, the exciton introduces a SPP decay channel and contributes to a third additional term k''_{jagg} to k''.[26] k''_{jagg} is expressed as

$$k''_{jagg} = \mathrm{Im}\left[\left(\frac{2\pi}{\lambda}\right)^2 \frac{\epsilon_{jagg}-1}{\epsilon_{jagg}} \left(\frac{|\epsilon'_m|}{|\epsilon'_m|-1}\right)^2 \frac{|\epsilon'_m|+\epsilon_{jagg}}{|\epsilon'_m|+1} \frac{d_{jagg}}{\sqrt{|\epsilon'_m|}}\right]. \tag{7}$$

In the above equation, ϵ_{jagg} and d_{jagg} are the complex permittivity $(\epsilon'_{jagg}+i\epsilon''_{jagg})$ of the *J*-aggregates and the thickness of the aggregate layer, respectively. Equation (7) is valid for values of d_{jagg} much smaller than the penetration depth of the SPP field in the air. The exponential decay of the SPP perpendicular to the interface can reach up to several hundreds of nanometers in air.[3] It is interesting to note that in Eq. (7), the losses are a linear function of the layer thickness, while the radiation losses at the metal/glass interface are exponentially depending on the thickness of the metal layer [see Eq. (2)].

In the resonance absorption, the aggregate permittivity can be approximated by a one electron oscillator model.[48,51] The real and imaginary parts of the permittivity can be written

$$\epsilon'_{jagg} = \epsilon_\infty + \left(\frac{4\pi e^2 N}{m}\right) \frac{\omega_0^2-\omega^2}{(\omega_0^2-\omega^2)+\Gamma^2\omega^2} \tag{8}$$

and

$$\epsilon''_{jagg} = \left(\frac{4\pi e^2 N}{m}\right) \frac{\Gamma\omega}{(\omega_0^2-\omega^2)+\Gamma^2\omega^2} \tag{9}$$

with the eigenfrequency ω_0 and the damping constant Γ. ϵ_∞ is the permittivity outside the resonance band. *e* and *m* are the electron charge and mass, respectively, and *N* is the number of oscillators per unit volume. We fitted the exciton peak of Fig. 5 with a Lorentzian curve and estimated Γ from the amplitude and the full-width at half-maximum of the resonance. We computed the value of ϵ'_{jagg} and ϵ''_{jagg} using Eqs. (8) and (9). We then calculated k'' by taking into account the intrinsic, radiative and absorption losses $k''_{\mathrm{int}}, k''_{\mathrm{rad}}$, and k''_{jagg}, respectively. The theoretical values of the damping constant L_{SP} are shown in Fig. 6 as the dashed curve. ϵ_∞ and d_{jagg} were kept as free parameters. The best agreement with the measured decay length was obtained for d_{jagg} and a silver film thickness of 30 nm. The discrepancy arising between the calculated silver thickness and the measured one can be reasonably explained by the relatively simple model we used. The molecular absorption of the dye was omitted in the model and only the absorption due to the *J*-aggregate formation was taken into account. Nonetheless, our model is well suited to predict the narrow damping of the SPP propagation as shown in Fig. 6.

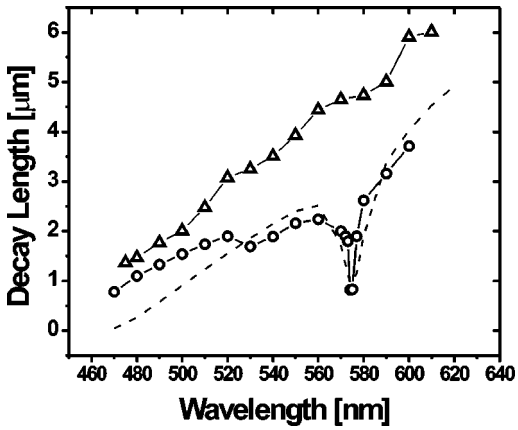

FIG. 6. Comparison of the surface plasmon propagation distance L_{SP} between an unmodified area of fresh 40-nm-thick silver film (triangles) and an area covered by *J* aggregates (circles). The dotted curve is the theoretical decay length computed by taking into account the surface plasmon losses of the silver film and the losses due to the excitonic absorption.

VII. CONCLUSION

In summary, we presented a far-field method to excite and observe surface plasmon intensity distribution through the detection of intrinsic leakage radiation. The plasmonic continuum spectroscopy (PCS) method permits the simultaneous excitation of a broad spectral distribution of surface plasmons. The SPPs form a directional streak with a rainbowlike color distribution. Observation of the SPP's leakage radiation gives a direct measurement of the propagation length of SPPs and the damping mechanisms for every wavelength in accordance with theoretical modeling. We found that radiation damping and the intrinsic losses are the main SPP damping processes and that roughness-induced attenuation has only a minor influence. We demonstrated the sensitivity of the surface plasmon propagation on changes of the dielectric environment and have shown that molecular excitonic aggregates can serve as an efficient surface plasmon rejection filter. We believe that this study is of importance for the next generation of plasmonic devices where surface plasmon-based information will need to be guided and transferred over some distances. We note that the excitation of a surface plasmon continuum using femtosecond white-light can also be accomplished by using a near-field aperture or a local scattering center to provide the necessary momentum spread.

ACKNOWLEDGMENTS

The authors express their gratitude to M. Firestone and Z. Saponjic for their advice in the preparation of the self-assembled monolayers. We thank the photosynthesis group for the use of the femtosecond laser. This work was supported by the Office of Basic Energy Sciences, Division of Materials Sciences, U.S. Department of Energy, under Contract No. W-31-109-ENG-38. This work also benefited from the Consortium for Nanoscience Research.

[1] For a review see J. Homola, S. Yee, and G. Gauglit, Sens. Actuators B **54**, 3 (1999).
[2] For a review see P. Schuck, Annu. Rev. Biophys. Biomol. Struct. **26**, 541 (1997).
[3] H. Raether, *Surface Plasmons* (Springer-Verlag, Berlin, 1988).
[4] E. Kretschmann and H. Raether, Z. Naturforsch. A **23**, 2135 (1968).
[5] L. A. Obando and K. S. Booksh, Anal. Chem. **71**, 5116 (1999).
[6] W. L. Barnes, A. Dereux, and T. W. Ebbesen, Nature (London) **424**, 824 (2003).
[7] P. Dawson, F. de Fornel, and J.-P. Goudonnet, Phys. Rev. Lett. **72**, 2927 (1994).
[8] S. I. Bozhevolnyi and F. A. Pudonin, Phys. Rev. Lett. **78**, 2823 (1997).
[9] J. C. Weeber, A. Dereux, Ch. Girard, J. R. Krenn, and J.-P. Goudonnet, Phys. Rev. B **60**, 9061 (1999).
[10] A. Bouhelier, Th. Huser, H. Tamaru, H.-J. Güntherodt, D. W. Pohl, F. I. Baida, and D. Van Labeke, Phys. Rev. B **63**, 155404 (2001).
[11] A. V. Shchegrov, I. V. Novikov, and A. A. Maradudin, Phys. Rev. Lett. **78**, 4269 (1997).
[12] I. I. Smolyaninov, D. L. Mazzoni, J. Mait, and Ch. C. Davis, Phys. Rev. B **56**, 1601 (1997).
[13] J. A. Sánchez-Gil, Appl. Phys. Lett. **73**, 3509 (1998).
[14] B. Hecht, H. Bielefeldt, L. Novotny, Y. Inouye, and D. W. Pohl, Phys. Rev. Lett. **77**, 1889 (1996).
[15] H. Ditlbacher, J. R. Krenn, G. Schider, A. Leitner, and F. R. Aussenegg, Appl. Phys. Lett. **81**, 1762 (2002).
[16] S. I. Bozhevolnyi, V. S. Volkov, and K. Leosson, Phys. Rev. Lett. **89**, 186801 (2002).
[17] J. Seidel, S. Grafström, L. Eng, and L. Bischoff, Appl. Phys. Lett. **82**, 1368 (2003).
[18] M. I. Stockman, Phys. Rev. Lett. **93**, 137404 (2004).
[19] J. Shoenvald, E. Busrtein, and M. Eslon, Solid State Commun. **12**, 185 (1973).
[20] D. L. Begley, D. A. Bryan, R. W. Alexander, and R. J. Bell, Appl. Opt. **16**, 1549 (1977).
[21] E. V. Elieva, G. Beitel, L. A. Kuzil, A. A. Sigarev, V. A. Yakoklev, G. N. Zhizhin, A. F. G. van der Meer, and M. J. van der Wiel, Appl. Spectrosc. **51**, 584 (1997).
[22] P. Dawson, B. A. F. Puygranier, and J.-P. Goudonnet, Phys. Rev. B **63**, 205410 (2001).
[23] J. J. Burke, G. I. Stegeman, and T. Tamir, Phys. Rev. B **33**, 5186 (1986).
[24] H. Tamaru, H. Ishikawa, and K. Miyano (unpublished).
[25] P. Dawson, G. Bryan-Brown, and J. R. Sambles, J. Mod. Opt. **41**, 1279 (1994).
[26] E. Kretschmann, Z. Phys. **241**, 313 (1971).
[27] D. L. Mills, Phys. Rev. B **12**, 4036 (1975).
[28] P. B. Johnson and R. W. Christy, Phys. Rev. B **6**, 4370 (1972).
[29] H. Hövel, S. Fritz, A. Hilger, U. Kreibig, and M. Vollmer, Phys. Rev. B **48**, 18 178 (1993).
[30] A. Henglein and D. Meisel, J. Phys. Chem. B **102**, 8364 (1998).
[31] T. T. Ehler, N. Malmberg, and L. J. Noe, J. Phys. Chem. B **101**, 1268 (1997).
[32] E. E. Jelley, Nature (London) **138**, 1009 (1936).
[33] G. Scheibe, Angew. Chem. **49**, 563 (1936).
[34] D. A. Higgins, P. J. Reid, and P. F. Barbara, J. Phys. Chem. **100**, 174 (1996).
[35] H. Fukumoto and Y. Yonezawa, Thin Solid Films **327-329**, 748 (1998).
[36] R. S. Eachus, A. P. Marchetti, and A. A. Muenter, Annu. Rev. Phys. Chem. **50**, 117 (1999).
[37] Y. Yamazaki, N. Tamai, T. Yamazaki, A. Murakami, M. Mimuro, and Y. Fujita, J. Phys. Chem. **92**, 5035 (1988).
[38] K. Minoshima, M. Taiji, K. Misawa, and T. Kobayashi, Chem. Phys. Lett. **218**, 67 (1994).
[39] F. C. Spano and S. Mukamel, J. Chem. Phys. **91**, 683 (1989).
[40] E. J. Sànchez, L. Novotny, and X. S. Xie, Phys. Rev. Lett. **82**, 4014 (1999).
[41] A. Bouhelier, M. R. Beversluis, and L. Novotny, Ultramicroscopy **100**, 413 (2004).
[42] M. Furuki, O. Wada, L. S. Pu, Y. Sato, H. Kawashima, and T. Tani, J. Phys. Chem. B **103**, 7607 (1999).
[43] K. Misawa and T. Kobayashi, J. Chem. Phys. **110**, 5844 (1999).
[44] R. Gagel and R. Gadonas, Chem. Phys. Lett. **217**, 228 (1994).
[45] H. Fidder, J. Terpstra, and D. A. Wiersma, J. Chem. Phys. **94**, 6895 (1991).
[46] V. Sundstrom, T. Gillbro, R. A. Gadonas, and A. Piskarkas, J. Chem. Phys. **89**, 2754 (1988).
[47] G. Wähling, D. Möbius, and H. Raether, Z. Naturforsch. A **33**, 907 (1978).
[48] G. Wähling, Z. Naturforsch. A **36**, 588 (1981).
[49] I. Pockrand, A. Brillante, and D. Möbius, Chem. Phys. Lett. **69**, 499 (1980).
[50] K. Saito, J. Phys. Chem. B **103** 6579 (1999).
[51] G. P. Wiederrecht, G. A. Wurtz, and J. Hranisavljevic, Nano Lett. **4**, 2121 (2004).
[52] D. A. Vanden Bout, J. Kerimo, D A. Higgins, and P. F. Barbara, Acc. Chem. Res. **30**, 204 (1997).